

Predictions for azimuthal anisotropy in Xe+Xe collisions at $\sqrt{s_{NN}} = 5.44$ TeV using a multiphase transport model

Sushanta Tripathy, Sudipan De, Mohammed Younus, and Raghunath Sahoo*

Discipline of Physics, School of Basic Sciences, Indian Institute of Technology Indore, Simrol, Indore 453552, India



(Received 29 April 2018; revised manuscript received 16 August 2018; published 10 December 2018)

Xe+Xe collision at relativistic energies may provide us with a partonic system whose size is approximately in between those produced by $p + p$ and Pb+Pb collisions. The experimental results on anisotropic flow in Xe+Xe and Pb+Pb collisions should provide us with an opportunity to study the system size dependence of v_2 . In the present work, we have used a multiphase transport model to calculate charged particles' v_2 for Xe+Xe collisions at $\sqrt{s_{NN}} = 5.44$ TeV. We have also tried to demonstrate the number of constituent quark, N_q , and m_T scaling of the elliptic flow. We find that n_q scaling of v_2 is not observed for the identified hadrons. The v_2 results from Xe+Xe collisions have also been compared to Pb+Pb collisions at $\sqrt{s_{NN}} = 5.02$ TeV. We find that flow of charged particles in (50–60)% central collisions for xenon nuclei is almost 30% less than particle flow developed in lead ion collisions, implying the important role the system size plays in the development of particle collective motion in relativistic heavy ion collisions.

DOI: [10.1103/PhysRevC.98.064904](https://doi.org/10.1103/PhysRevC.98.064904)

I. INTRODUCTION

The main goal of the ultrarelativistic heavy-ion collisions is to study the matter at high temperature and density where quantum chromodynamics predict the existence of the quark-gluon plasma (QGP) [1] under such extreme conditions. The BNL Relativistic Heavy Ion Collider (RHIC) and CERN Large Hadron Collider (LHC) are the dedicated state-of-the-art experimental facilities to this end and are focused to understand the properties of QGP. Anisotropic flow as an observable of QGP is caused by the initial asymmetries in the geometry of the system produced in any noncentral collision, and plays an important role to understand the collective motion and bulk property of the QGP. The elliptic flow or azimuthal anisotropy (v_2), which is defined as the second-order Fourier component of the particle azimuthal distribution provides information about the equation of state, initial geometrical anisotropy, and the transport properties of created QGP [2]. The elliptic flow has been intensively studied at RHIC and LHC for different systems like Au+Au, Cu+Cu, and Pb+Pb at different center of mass energies from 7.7 GeV to 5.02 TeV. From many of the measurements from these previous experiments we have seen that v_2 has contributed significantly to the characterization of the system created in heavy-ion collisions as it is sensitive to the properties of

the system at an early time of its evolution. Earlier RHIC experiments show that at low transverse momentum (p_T) region ($p_T < 2$ GeV/ c), v_2 follows the mass ordering, i.e., higher mass particles having lower v_2 values [3–10]. Another important feature of v_2 is the number of constituent quark (NCQ) scaling, where v_2 and p_T of identified hadrons are divided by the number of constituent quarks (n_q). This scaling interprets the dominance of the quark degrees of freedom at early stages of the collision. Recently LHC has shown similar mass ordering of v_2 at low- p_T but it seems that v_2 does not follow the NCQ scaling at LHC energies [11,12] for intermediate or high momentum. It would be very interesting to study these properties of v_2 in QGP medium with varying spatial configurations and densities, etc., of partons, which can be achieved by relativistic collisions of different species of ions with a large variation of mass number at same center of mass energy.

Recently LHC has collided Xe¹²⁹ nuclei at $\sqrt{s_{NN}} = 5.44$ TeV. Since the mass number of the Xe¹²⁹ nuclei is roughly in the middle proton and Pb²⁰⁸ nuclei, this can provide the unique opportunity to study the system-size dependence of elliptic flow at LHC energies. According to the recent hydrodynamical calculation [13], v_2 is found larger by 25% in Xe+Xe than in Pb+Pb collisions in 0–5% centrality class but it is smaller by 10% above 30% centrality classes. An earlier prediction from a multiphase transport (AMPT) model suggests that the NCQ scaling will hold when we consider much smaller system than Pb+Pb, which has shown that the number of constituent quarks (NCQ), n_q scaling holds for Si+Si collisions at $\sqrt{s_{NN}} = 2.76$ TeV much better than that of Pb+Pb collisions at the same energy [14]. Hence, It is also expected that NCQ scaling will also hold true for v_2 in Xe+Xe collisions. As expected, this may also indicate the formation of partonic system in xenon nuclei collisions

*Corresponding author: Raghunath.Sahoo@cern.ch

Published by the American Physical Society under the terms of the [Creative Commons Attribution 4.0 International](https://creativecommons.org/licenses/by/4.0/) license. Further distribution of this work must maintain attribution to the author(s) and the published article's title, journal citation, and DOI. Funded by SCOAP³.

similar to Au+Au or Pb+Pb collisions. Therefore the study of v_2 will be very interesting at LHC energies with smaller system size. In this article we have studied the v_2 of produced particles in Xe+Xe collisions at $\sqrt{s_{NN}} = 5.44$ TeV using AMPT model with string melting version [15,16].

The paper is organized as follows. The next section briefly deals with the AMPT model we are using to calculate v_2 of charged particles. This is followed by a section on results and their discussion. We then conclude our paper by summarizing our results and findings in the conclusions.

II. A MULTI-PHASE TRANSPORT (AMPT) MODEL

AMPT is a hybrid transport model which contains four components, namely, initialization of collisions, parton transport after initialization, hadronization mechanism, and hadron transport [17]. The initialization of the model follows the HIJING model [18] and calculates the differential cross section of the produced minijet particles in $p + p$ collisions which is given by

$$\frac{d\sigma}{dp_T^2 dy_1 dy_2} = K \sum_{a,b} x_1 f_a(x_1, p_{T1}^2) x_2 f_b(x_2, p_{T2}^2) \times \frac{d\hat{\sigma}_{ab}}{d\hat{t}}, \quad (1)$$

where σ is the produced particles cross section and \hat{t} is the momentum transfer during partonic interactions in $p + p$ collisions. x_i 's are the momentum fraction of the mother protons which are carried by interacting partons and $f(x, p_T^2)$'s are the parton density functions (PDF). The produced partons calculated in $p + p$ collisions are then converted into $A + A$ and $p + A$ collisions by incorporating the parametrized shadowing function and nuclear overlap function using the in-built Glauber model within HIJING. Similarly, initial low-momentum partons which are separated from high momenta partons by momentum cut-off, are produced from parametrized colored string fragmentations mechanisms. The produced particles are initiated into parton transport part, Zhang Parton Cascade (ZPC) [19], which transport the quarks and gluons using the Boltzmann transport equation which is given by

$$p^\mu \partial_\mu f(x, p, t) = C[f]. \quad (2)$$

The leading order equation showing interactions among partons is approximately given by

$$\frac{d\hat{\sigma}_{gg}}{d\hat{t}} \approx \frac{9\pi\alpha_s^2}{2(\hat{t} - \mu^2)^2}. \quad (3)$$

Here, σ_{gg} is the gluon scattering cross section, α_s is the strong coupling constant used in above equation, and μ^2 is the cutoff used to avoid infrared divergences which can occur if the momentum transfer, \hat{t} , goes to zero during scattering. In the string melting version of AMPT (AMPT-SM), melting of colored strings into low-momentum partons also take place at the start of the ZPC and are calculated using the Lund FRITIOF model of HIJING. This melting phenomenon depends upon the spin and flavor of the excited strings. The resulting partons undergo multiple scatterings which take place when any two

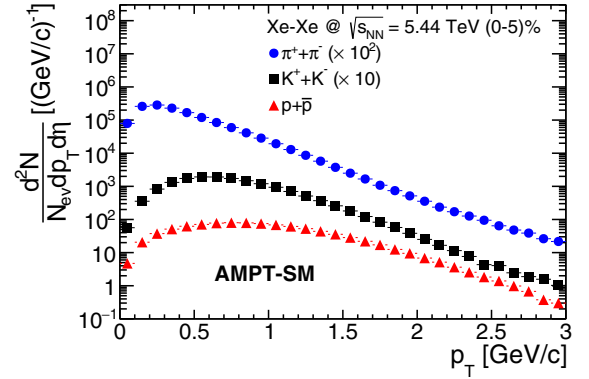


FIG. 1. p_T spectra of π , K , and p for (0–5)% centrality in Xe+Xe collisions. Circles are for pions, squares stand for kaons, and triangles represent protons. The vertical lines in data points show the statistical uncertainties.

partons are within distance of minimum approach which is given by $d \leq \sqrt{\sigma/\pi}$, where σ is the scattering cross section of the partons. In AMPT-SM, the transported partons are finally hadronized using coalescence mechanism [20], when two (or three) quarks sharing a close phase-space combine to form a meson (or a baryon). As of present, AMPT-SM uses three-momentum conservation and the invariant masses of the coalescing partons. The coalescence takes place using the following equation (for e.g. meson):

$$\frac{d^3N}{d^3p_M} = g_M \int d^3x_1 d^3x_2 d^3p_1 d^3p_2 f_q(\vec{x}_1, \vec{p}_1) f_{\bar{q}}(\vec{x}_2, \vec{p}_2) \times \delta^3(\vec{p}_M - \vec{p}_1 - \vec{p}_2) f_M(\vec{x}_1 - \vec{x}_2, \vec{p}_1 - \vec{p}_2). \quad (4)$$

Here, g_M is the meson degeneracy factor, f_q 's are the quark distributions after the evolution, and f_M is the coalescing function commonly called Wigner functions [21].

The produced hadrons further undergo evolution in the A Relativistic Transport model (ART) mechanism [22,23] via meson-meson, meson-baryon, and baryon-baryon interactions, before final spectra can be observed. There is another default version of AMPT known as AMPT-Def where instead of coalescing the partons, the fragmentation mechanism using Lund fragmentation parameters a and b are used for hadronizing the transported partons. However, it is believed that particle flow and spectra at the mid- p_T regions are well explained by the quark coalescence mechanism for hadronization [21,24,25]. We have used the AMPT-SM mode for our calculations. We have used the AMPT version 2.26t7 (released 10/28/2016) in our current work.

Before we start discussing v_2 , it is important to have a look into the p_T spectra of the produced particles such as π , K , and p . Figure 1 shows p_T spectra of π , K , and p for (0–5)% centrality. The error bars in the data points are the statistical uncertainties. The spectra of pions and kaons are multiplied by different constant factors to get a clear view of each spectrum. This provides a very good baseline to study the p_T spectra of identified particles in experiment for Xe+Xe collisions.

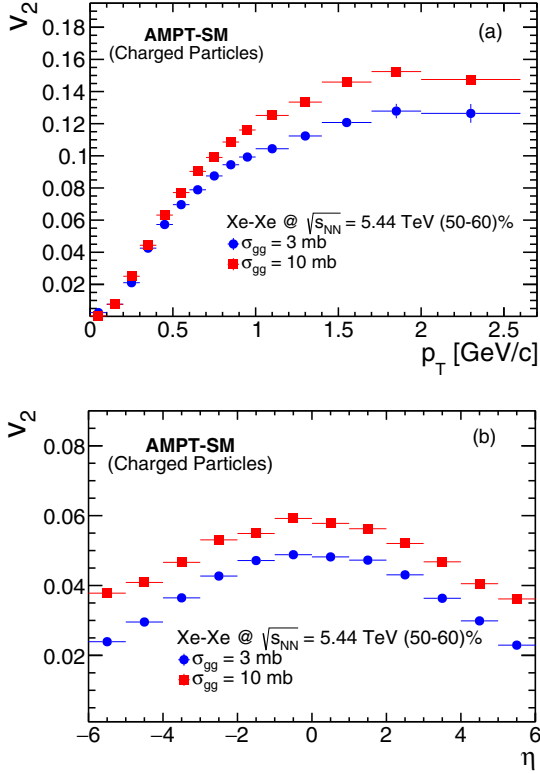


FIG. 2. Charged particles v_2 vs transverse momentum, p_T (a), and pseudorapidity, η (b). Different symbols are for $\sigma_{gg} = 3$ mb and 10 mb.

It is worthwhile to mention that earlier studies of particle v_2 in Pb+Pb collisions with AMPT showed a greater match with experimental data when a large partonic scattering cross section ($\sigma_{gg} \approx 10$ mb) is taken [26]. In Fig. 2, we have shown the azimuthal anisotropy or elliptic flow of charged particles, v_2 , as functions of transverse momentum, p_T , and rapidity, η for two values of scattering cross sections, $\sigma_{gg} = 3$ mb and 10 mb. As expected, results with 10 mb show greater v_2 than 3 mb. In the case of p_T as a variable, the flow increases more with transverse momentum in the 10 mb scenario than 3 mb. While, taking rapidity, η , as the variable, the difference in 10 mb and 3 mb results can be seen as a constant multiplication factor, particularly in the central rapidity region. In the present work we have fixed $\sigma_{gg} = 10$ mb as a cross section for our calculations and calculated charged particle v_2 . The Lund string fragmentation parameters a and b are kept fixed at their default values of 2.2 and 0.5/GeV², respectively. We will compare our results with the experimental data when they become available and further optimize the parameters.

The anisotropic flow can be characterized by the coefficients (v_n), which are obtained from a Fourier expansion of the momentum distribution of the charged particles and is given by

$$E \frac{d^3 N}{d^3 p} = \frac{d^2 N}{2\pi p_T dp_T dy} \left(1 + 2 \sum_{n=1}^{\infty} v_n \cos[n(\phi - \psi_n)] \right), \quad (5)$$

where ϕ is the azimuthal angle in the transverse momentum plane and ψ_n is the n th harmonic event plane angle [11]. In the current work elliptic flow is calculated with respect to the reaction plane by taking $\psi_n = 0$, which implies that the event plane coincides with the reaction plane. Taking $n = 2$ gives the second-order harmonics in the expansion and its coefficient v_2 is calculated to provide the measure of the elliptic flow or azimuthal anisotropy. For a given rapidity window the v_2 is defined as

$$v_2 = \langle \cos(2\phi) \rangle \quad (6)$$

For noncentral collisions the v_2 should be a nonzero finite quantity.

III. RESULTS AND DISCUSSIONS

We have calculated charged particles elliptic flow or azimuthal anisotropy, v_2 , for various centralities, namely, (0–5)%, (10–20)%, (20–30)%, (50–60)%, (60–70)% centrality classes. Results are presented for $0 < p_T < 2.7$ GeV/c in midrapidity region ($|\eta| < 0.8$). It is believed that the Xe nucleus is moderately deformed. Earlier theoretical studies [13] on central collisions [$\approx(0-15\%)$] of Xe nuclei have shown that incorporating deformation parameters cause about 15% deviation in v_2 compared to nondeformed cases. Beyond 15% centrality, it is claimed that the deformity has no discernible effects on particle spectra or other observables. In the present work as the first approximation, we have not used any deformation for xenon nuclei. Most of the results are shown for the above-mentioned centralities for Xe+Xe collisions at $\sqrt{s_{NN}} = 5.44$ TeV.

In Fig. 3, we have shown the elliptic flow of charged particles for six different centralities. For the most central collision (0–5%), the calculated v_2 is minimum. The elliptic flow increases as the centrality is increased as evident from the next three centralities [(10–20)%, (20–30)%, and (30–40)%] shown in the figure. However we see that the difference between (20–30)% and (30–40)% is small. In (50–60)% onwards, we have a decreasing trend in the flow and smaller v_2 , which continues to decrease for more peripheral collisions. We feel that this might be due to formation of a smaller system in peripheral collisions at which, although we have more geometrical anisotropy, the medium density is very small and probability of formation of collective motion decreases.

Figure 4 shows transverse momentum integrated v_2 with the centrality in the p_T range mentioned above. As expected, a strong dependence of v_2 with centrality is observed. It is quite evident from this figure that v_2 increases from most central to midcentral collisions. Beyond that as we move towards peripheral collisions the flow decreases rapidly. Similar behavior of the charged particle elliptic flow has also been observed for Pb-Pb collisions at LHC energies [27]. Earlier calculations with hydrodynamical models give similar pictures of elliptic flow with centrality. However, our calculations underestimate the results of hydrodynamics roughly by (13–30)% [13]. We will continue to optimize the AMPT parameters like σ_{gg} , a , and b in accordance with the upcoming experimental data and study the centrality dependencies of particle flow for Xe nuclei collisions in our future works, which in turn will help

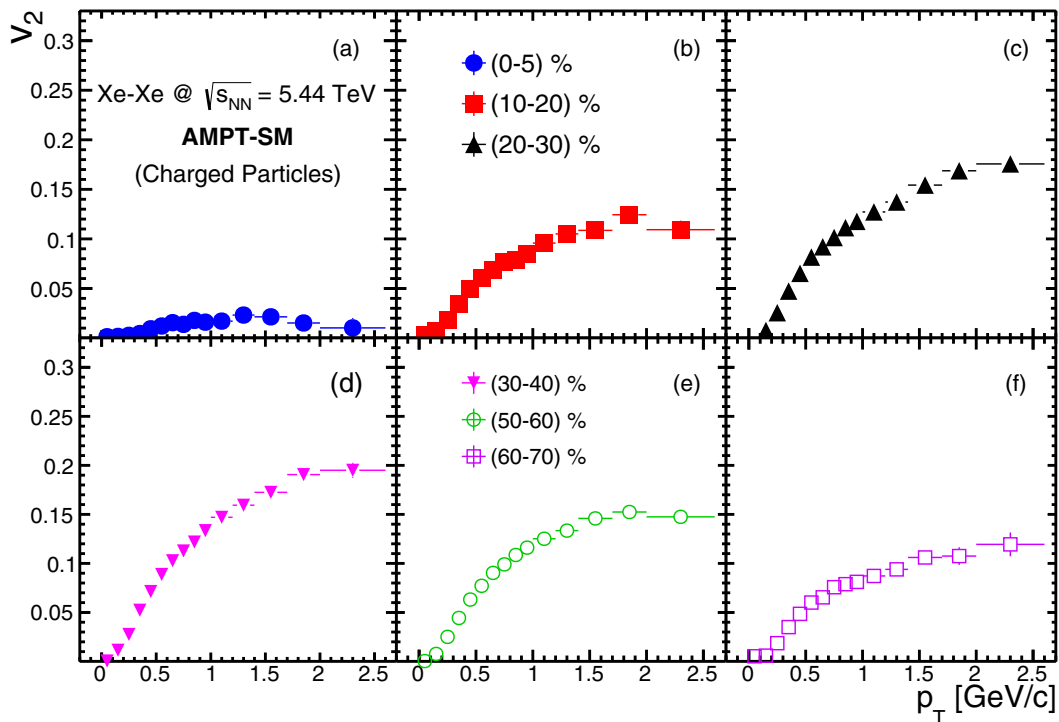


FIG. 3. Charged particles v_2 as a function of transverse momentum, p_T for different centrality classes. Different sections of the figure represent different centrality bins starting from (0–5)% (a) to (60–70)% (f).

in studying other observables of greater importance in order to characterize the systems formed in Xe+Xe collisions. However, the recent experimental data do not have results beyond 70% centrality. The statistics are too low. With a purpose to study the effects of anisotropy at the peripheral collisions with sufficient statistics, we have used a big centrality range of 70–100%. The v_2 shows a very small value at most peripheral collisions in AMPT scenario. We feel that although the spatial anisotropy is largest for the peripheral collisions, the medium density is too small to provide any collective flow effects and the interactions among partons are less.

In Fig. 5, we have compared v_2 of charged particles in Pb+Pb collisions at $\sqrt{s_{NN}} = 5.02$ TeV with Xe+Xe collisions at $\sqrt{s_{NN}} = 5.44$ TeV at midrapidity ($|\eta| < 0.8$) using

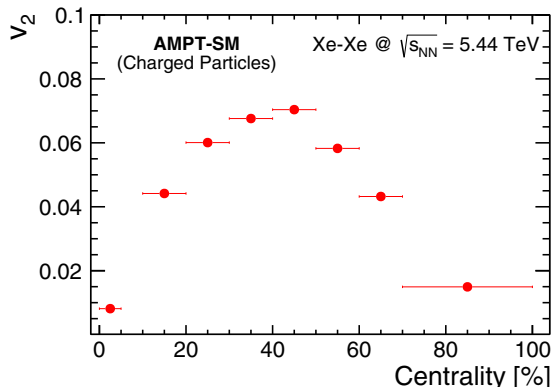


FIG. 4. Charged particles v_2 vs centrality for $|\eta| < 0.8$.

the same configurations in the AMPT model. The available collisions energies for these two different systems are close to each other and hence we may be able to discern various properties of QGP which depend on system sizes. The dependence of elliptic flow on the system size is quite evident from the plot, as v_2 from Xe+Xe is always different from Pb+Pb collisions. For (50–60)% centrality, the anisotropic flow is more in Pb system than that of Xe. The difference increases toward higher p_T and around 30% higher v_2 is observed in the Pb system. We would like to reiterate that inclusion of

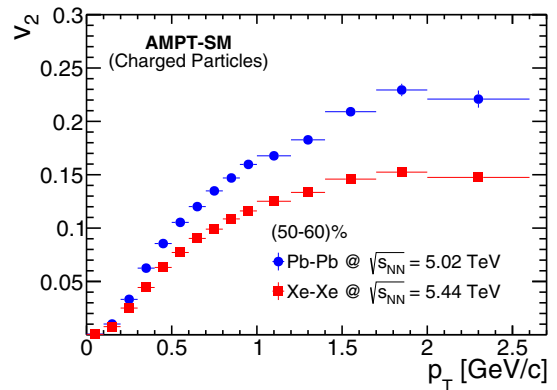


FIG. 5. Charged particles v_2 vs transverse momentum, p_T for (50–60)% centrality of Pb+Pb and Xe+Xe collisions. Circles are for Pb+Pb collisions at $\sqrt{s_{NN}} = 5.02$ TeV and squares are for Xe+Xe collisions at $\sqrt{s_{NN}} = 5.44$ TeV. The vertical lines in data points show the statistical uncertainties.

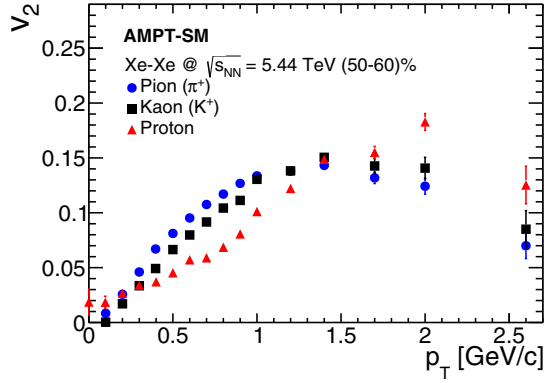


FIG. 6. v_2 vs transverse momentum, p_T of π , K and p for (50–60)% centrality in Xe+Xe collisions. Circles are for pions, squares stand for kaons, and triangles represent protons. The vertical lines in data points show the statistical uncertainties.

intrinsic deformations for xenon nuclei in the calculations may change many of the above features of observables and their comparative studies. We will continue to investigate this particular feature and report in our future works.

Figure 6 shows v_2 for π , K , and p up to $p_T = 2.7$ GeV/ c for (50–60)% centrality. A clear mass dependency of hadrons' $v_2(p_T)$ is observed for $p_T < 2$ GeV/ c as it has been observed in Pb-Pb collisions [11,27] earlier. Lower mass particles have higher v_2 . In particular, the pions and kaons show slightly more flow than proton for $p_T < 2.0$ GeV/ c , whereas afterwards the proton takes over the pions and kaons. According to the hydrodynamical calculations there is an interplay between radial and elliptic flow which may play an important role in determining this mass ordering of v_2 at low- p_T . For $p_T > 2$ GeV/ c v_2 is separated according to baryons and mesons. The quark-coalescence mechanism, [21,24] which is able to explain flow at the intermediate or moderate p_T ranges has been considered for hadronization in AMPT-SM model used in our calculations.

Within AMPT mechanisms, when a quark and an antiquark are close in phase space with their momenta very close to each other, they coalesce to form a meson. Similarly when three quarks come closer in phase space, they recombine to form a baryon. Since we assume that the coalescence mechanism should work in the intermediate p_T region, the calculated elliptic flow of charged hadrons when divided by their coalesced constituent quark numbers may exhibit n_q scaling behavior. In Fig. 7(a), we have shown a number of constituent quarks, n_q , scaling of v_2 for π , K , and p for (50–60)% centrality. In the present work, it is calculated as

$$v_2^h(p_T) = n_q \cdot v_2^q(p_T/n_q), \quad (7)$$

where n_q is the number of constituent quarks for the charged hadrons considered in our work. However, the figure does not demonstrate the n_q scaling behavior. We observe that scaled v_2 for protons does not match with those of mesons, π and K . Such violation of n_q scaling has been observed for charged particles v_2 in Pb+Pb collisions at the LHC energies [11]. In Fig. 7(b), we tried to demonstrate n_q scaling of the particles flow, where instead of p_T along the x axis, we have

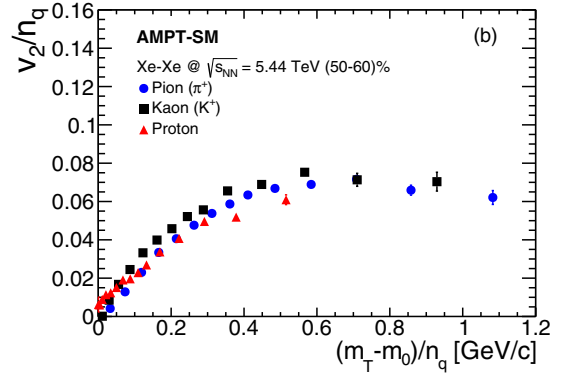
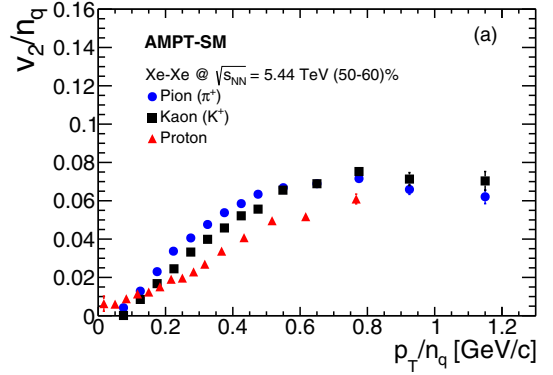


FIG. 7. (a) v_2/n_q as a function of p_T/n_q for π , K , and p . (b) v_2/n_q as a function of $(m_T - m_0)/n_q$ for π , K , and p . Both plots are for 50–60% centrality bin and different symbols represent different particles. The vertical lines in data points show the statistical uncertainties.

$(m_T - m_0)/n_q$, where $m_T = \sqrt{p_T^2 + m_0^2}$. We find that the v_2/n_q values as a function of $(m_T - m_0)/n_q$ show a scaling-like behavior which is similar to the observations for Pb+Pb collisions at LHC energies [11]. However, we cannot state conclusively that n_q scaling is observed although something similar to m_T scaling can be seen at low momenta. The reason behind the failed n_q scaling may be due to the partons forming baryons occupying different phase space as compared to partons forming mesons. The study of the correlation of the relaxation and freeze-out times with the flow may shed some light on the difference in the flow among quarks at the partonic level [28]. This calls for a more deeper understanding of the relaxation of the bulk system of quarks and gluons.

IV. SUMMARY

Xe+Xe collisions may provide us with a partonic system whose size is approximately in between those produced by $p + p$ and Pb+Pb collisions. The experimental results on anisotropic flow in Xe+Xe and Pb+Pb collisions should provide us with an opportunity to study system size dependence of v_2 at the approximately same collision energies. In the present work we have used AMPT-SM model to calculate charged particles' v_2 for Xe+Xe collisions at $\sqrt{s_{NN}} = 5.44$ TeV at midrapidity region $|\eta| < 0.8$ in $0 < p_T < 2.7$ GeV/ c . A strong centrality dependence of the v_2 is observed.

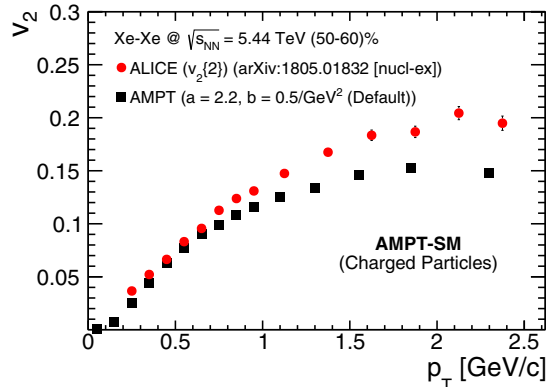


FIG. 8. v_2 vs transverse momentum, p_T of charged particles for ALICE data [29] (circles) and AMPT-SM model (squares).

p_T differential v_2 is measured for identified particles such as, pions, kaons, and protons and a clear mass ordering is observed for $p_T < 2$ GeV/c. We have also tried to demonstrate the number of constituent quarks, n_q of the elliptic flow as a function of p_T/n_q as well as with respect to $(m_T - m_0)/n_q$. We find that n_q scaling of v_2 is not observed for types of charged particles used for our studies. Also we have not used any intrinsic deformations as a first approximation referring to earlier works, which suggest its small influence on observed particle spectra and v_2 beyond 15% centrality collisions. However, most of the results are presented for (50–60)% centrality bin where we do not expect the effects due to deformations. AMPT-SM underestimates the experimental results at higher p_T ($p_T > 1$ GeV/c) with default parameters. It suggests that one needs to tune the parameters to reproduce

the experimental results. This study provides a baseline for the recent experimental results. This is discussed in the Appendix.

ACKNOWLEDGMENTS

The authors acknowledge the financial supports from ALICE Project No. SR/MF/PS-01/2014-IITI(G) of Department of Science and Technology, Government of India. S.T. acknowledges the financial support by DST-INSPIRE program of Government of India. This research used resources of the LHC grid computing centers at Variable Energy Cyclotron Center, Kolkata.

APPENDIX

Recently ALICE has published the v_2 measurements of charged particles in Xe+Xe collisions at $\sqrt{s_{NN}} = 5.44$ TeV [29] using two-particle correlations based on the cumulant method [30]. Figure 8 shows the comparison of v_2 vs p_T between data and AMPT-SM model for 50–60% centrality bin. It is found that AMPT result matches with data well at low- p_T region ($p_T < 1$ GeV/c). The difference between data and AMPT increases as we go towards higher p_T . As there were no experimental results available before, we took the default parameter settings of AMPT-SM as is mentioned in Sec. II. It seems that to reproduce these latest experimental results, particularly at higher p_T , one needs to tune the parameters of AMPT-SM model. It should be noted here that the methods adopted in this paper and in the ALICE experimental paper for the measurement/estimation of v_2 are different. We have used the event plane method, whereas the experimental measurement uses the cumulant method. However, as discussed in Ref. [30] both the methods give similar v_2 results.

-
- [1] S. A. Bass, M. Gyulassy, H. Stoecker, and W. Greiner, *J. Phys. G* **25**, R1 (1999).
- [2] S. Voloshin and Y. Zhang, *Z. Phys. C* **70**, 665 (1996).
- [3] J. Adams *et al.* (STAR Collaboration), *Phys. Rev. Lett.* **92**, 052302 (2004).
- [4] B. I. Abelev *et al.* (STAR Collaboration), *Phys. Rev. C* **75**, 054906 (2007).
- [5] J. Adams *et al.* (STAR Collaboration), *Phys. Rev. C* **72**, 014904 (2005).
- [6] B. I. Abelev *et al.* (STAR Collaboration), *Phys. Rev. Lett.* **99**, 112301 (2007).
- [7] S. S. Adler *et al.* (PHENIX Collaboration), *Phys. Rev. Lett.* **91**, 182301 (2003).
- [8] S. Afanasiev *et al.* (PHENIX Collaboration), *Phys. Rev. Lett.* **99**, 052301 (2007).
- [9] A. Adare *et al.* (PHENIX Collaboration), *Phys. Rev. Lett.* **98**, 162301 (2007).
- [10] A. Adare *et al.* (PHENIX Collaboration), *Phys. Rev. C* **85**, 064914 (2012).
- [11] B. B. Abelev *et al.* (ALICE Collaboration), *J. High Energy Phys.* **06** (2015) 190.
- [12] K. Aamodt *et al.* (ALICE Collaboration), *Phys. Rev. Lett.* **105**, 252302 (2010).
- [13] G. Giacalone, J. Noronha-Hostler, M. Luzum, and J. Y. Ollitrault, *Phys. Rev. C* **97**, 034904 (2018).
- [14] S. Singha and M. Nasim, *Phys. Rev. C* **93**, 034908 (2016).
- [15] Z. W. Lin and C. M. Ko, *Phys. Rev. C* **65**, 034904 (2002).
- [16] L. W. Chen, V. Greco, C. M. Ko, and P. F. Kolb, *Phys. Lett. B* **605**, 95 (2005).
- [17] Z. W. Lin, C. M. Ko, B. A. Li, B. Zhang, and S. Pal, *Phys. Rev. C* **72**, 064901 (2005).
- [18] X. N. Wang and M. Gyulassy, *Phys. Rev. D* **44**, 3501 (1991).
- [19] B. Zhang, *Comput. Phys. Commun.* **109**, 193 (1998).
- [20] V. Greco, C. M. Ko, and P. Levai, *Phys. Rev. Lett.* **90**, 202302 (2003).
- [21] V. Greco, C. M. Ko, and P. Levai, *Phys. Rev. C* **68**, 034904 (2003).
- [22] B. Li, A. T. Sustich, B. Zhang, and C. M. Ko, *Int. J. Mod. Phys. E* **10**, 267 (2001).
- [23] B. A. Li and C. M. Ko, *Phys. Rev. C* **52**, 2037 (1995).
- [24] R. J. Fries, B. Muller, C. Nonaka, and S. A. Bass, *Phys. Rev. Lett.* **90**, 202303 (2003).
- [25] R. J. Fries, B. Muller, C. Nonaka, and S. A. Bass, *Phys. Rev. C* **68**, 044902 (2003).

- [26] Z. Feng, G. M. Huang, and F. Liu, *Chin. Phys. C* **41**, 024001 (2017).
- [27] L. Zheng *et al.*, *Eur. Phys. J. A* **53**, 124 (2017).
- [28] M. Younus, S. Tripathy, S. K. Tiwari, and R. Sahoo, [arXiv:1803.01578](https://arxiv.org/abs/1803.01578) (2018).
- [29] S. Acharya *et al.* (ALICE Collaboration), *Phys. Lett. B* **784**, 82 (2018).
- [30] A. Bilandzic, R. Snellings, and S. Voloshin, *Phys. Rev. C* **83**, 044913 (2011).